



Exciton linewidth broadening induced by exciton–phonon interactions in CsPbBr₃ nanocrystals

Cite as: J. Chem. Phys. **154**, 214502 (2021); <https://doi.org/10.1063/5.0051611>

Submitted: 26 March 2021 . Accepted: 14 May 2021 . Published Online: 01 June 2021

Buyang Yu,  Chunfeng Zhang, Lan Chen, Xinyu Huang, Zhengyuan Qin,  Xiaoyong Wang,  Min Xiao, et al.

COLLECTIONS

Paper published as part of the special topic on [Coherent Multidimensional Spectroscopy](#)



View Online



Export Citation



CrossMark

ARTICLES YOU MAY BE INTERESTED IN

[Size-dependent dark exciton properties in cesium lead halide perovskite quantum dots](#)

The Journal of Chemical Physics **153**, 184703 (2020); <https://doi.org/10.1063/5.0027972>

[Exciton-phonon coupling in a CsPbBr₃ single nanocrystal](#)

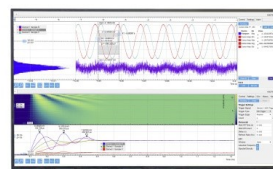
Applied Physics Letters **112**, 072104 (2018); <https://doi.org/10.1063/1.5018413>

[Coherent exciton-phonon coupling in perovskite semiconductor nanocrystals studied by two-dimensional electronic spectroscopy](#)

Applied Physics Letters **115**, 243101 (2019); <https://doi.org/10.1063/1.5130636>

Challenge us.

What are your needs for
periodic signal detection?



Zurich
Instruments



Exciton linewidth broadening induced by exciton–phonon interactions in CsPbBr₃ nanocrystals

Cite as: J. Chem. Phys. 154, 214502 (2021); doi: 10.1063/5.0051611

Submitted: 26 March 2021 • Accepted: 14 May 2021 •

Published Online: 1 June 2021



View Online



Export Citation



CrossMark

Buyang Yu,¹ Chunfeng Zhang,^{1,a)} Lan Chen,¹ Xinyu Huang,¹ Zhengyuan Qin,¹ Xiaoyong Wang,¹ and Min Xiao^{2,b)}

AFFILIATIONS

¹National Laboratory of Solid State Microstructures, School of Physics, and Collaborative Innovation Center for Advanced Microstructures, Nanjing University, Nanjing 210093, China

²Department of Physics, University of Arkansas, Fayetteville, Arkansas 72701, USA

Note: This paper is part of the JCP Special Topic on Coherent Multidimensional Spectroscopy.

^{a)}Author to whom correspondence should be addressed: cfzhang@nju.edu.cn

^{b)}E-mail: mxiao@uark.edu

ABSTRACT

Quantum dephasing of excitonic transitions in CsPbBr₃ nanocrystals has been studied using two-dimensional electronic spectroscopy at cryogenic temperatures. The exciton–phonon interactions for acoustic and optical modes exhibit different effects on the coherent dynamics of excitonic transitions. The homogeneous linewidth shows a proportional dependence on the temperature, suggesting the primary dephasing channel of the elastic scattering between exciton and acoustic modes. The exciton–optical mode interaction is manifested as the beatings of off-diagonal signals in the population time domain at the frequencies of 29 and 51 cm⁻¹, indicating phonon replicas of excitonic transitions arising from coherent exciton–phonon interaction. The insight information of exciton homogeneous broadening in perovskite nanocrystals is essential for the potential application of quantum light sources.

Published under an exclusive license by AIP Publishing. <https://doi.org/10.1063/5.0051611>

I. INTRODUCTION

Perovskite semiconductors have emerged as a promising family of materials for optoelectronic applications^{1–3} due to their strong light absorption^{4–6} and excellent charge transport properties.^{7–9} When the size decreases to the scale comparable to or smaller than the Bohr radius, photon absorption in these perovskite nanocrystals will create excitons with spatially confined electron and hole wavefunctions.^{10,11} Benefiting from the quantum confinement effect, excitons in perovskite nanocrystals exhibit narrow spectral characteristics, which promote the light-emitting properties for applications such as lasers^{12–15} and light-emitting diodes.^{16–20}

Excitonic transitions in perovskite nanocrystals have also been demonstrated as quasi two-level systems with excellent single photon emissions,^{21–24} which can be potentially applied as coherent

light sources for quantum information technology. In general, the homogeneous linewidth of a two-level system is limited by the system–bath interaction. The solid system of semiconductor nanocrystals is markedly different from the atom gases because of the interaction between the exciton and lattice vibration. Elucidating the intrinsic linewidths and the underlying broadening mechanisms is essential to understand the coherent light emission properties in perovskite nanocrystals.

The spectral linewidths in perovskite nanocrystals have been recently studied using single-nanocrystal photoluminescence (PL) spectroscopic experiments.^{25–27} Nevertheless, due to dot-to-dot variation, it is challenging to fully survey the homogeneous linewidth in nanocrystal ensembles. For nanocrystal ensembles, temporal four-wave mixing has been conducted to study the mechanism of dephasing in perovskite nanocrystals, which provides no information about its variation across the inhomogeneous

distribution induced by the size and shape dispersion.²⁸ Broadband two-dimensional electronic spectroscopy (2DES) can address the above issues by correlating excitation and emission spectra and thus disentangle the inhomogeneous and homogeneous broadening. 2DES has been successfully applied to investigate the exciton fine states, lineshape dynamics, and biexciton interactions in perovskite nanostructures.^{29–32}

In this work, we investigate the mechanism of exciton homogeneous broadening in CsPbBr₃ perovskite nanocrystals, emphasizing the effect of the exciton–phonon interaction using 2DES measurements. Using temperature-dependent 2DES measurements, we observe that the homogeneous linewidth increases proportionally with increasing temperature in the range of 6–40 K, suggesting an important dephasing pathway induced by the elastic scattering between exciton and acoustic phonons. In addition, the off-diagonal feature and the beatings in population time suggest the phonon replicas of excitonic transitions for two optical phonon modes of 29 and 51 cm⁻¹. The findings suggest different important roles played by the interactions between exciton and acoustic or optical phonons in coherent light emissions, which is instrumental for the future design of perovskite nanocrystal-based quantum light sources.

II. METHODS

A. Sample preparations

The synthesis of colloidal CsPbBr₃ nanocrystals has previously been described in detail.¹⁰ In brief, Cs₂CO₃ (0.8 g, 99%, Sigma-Aldrich) and oleic acid (2.5 ml, 90%, Sigma-Aldrich) were dissolved in octadecene (30 ml, 90%, Sigma-Aldrich) at 150 °C to synthesize the Cs-oleate precursor. PbBr₂ (0.138 g, 98%, Sigma-Aldrich) was dissolved in octadecene (10 ml) at 180 °C with a 1:1 mixture of oleylamine (1 ml, 70%, Sigma-Aldrich) and oleic acid (1 ml). The 100 °C Cs-oleate precursor was quickly injected into the PbBr₂ solution, and the reaction time was controlled for 5 s before being placed in an ice-water bath. Then, the synthesized nanocrystals were washed by ethylacetate and dispersed in hexane solvent. The average edge length of the synthesized CsPbBr₃ nanocrystals is ~8.8 nm. A drop-cast film with wedgy sapphire substrates was prepared for the 2DES measurements. The thickness of the nanocrystal film is ~120 nm.

B. Experimental details

The 2DES setup is based on a pump–probe geometry with active phase stabilization.³³ Two home-made non-collinear optical parametric amplifiers (NOPAs) were exploited as pump and probe sources. The beam (800 nm, 90 fs, 1 kHz) of a Ti:sapphire regenerative amplifier (Libra, Coherent) was employed to pump NOPAs. The pulse sequence of 2DES is shown in Fig. 1(a) where two phase-locked replica of pump NOPAs with time delay τ split from the pump beam and re-combined to excite the sample. The probe beam was delayed by a population time T after the second pump pulse. In our configuration, a fiber spectrometer (Maya 2000 Pro, Ocean Optics) was used to monitor the phase difference between the two pump beams. The transmitted probe pulse was collected by a monochromator (SpectraPro HRS-750, Princeton Instruments) and

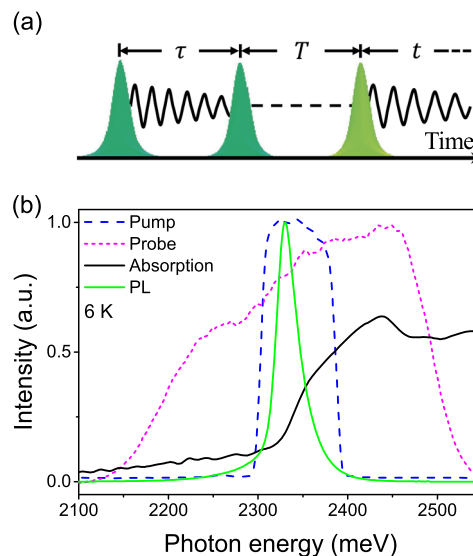


FIG. 1. (a) Schematic diagram of the pulse sequence used in 2DES measurements. Delays between the three incident pulses and the signal are denoted as τ , T , and t , respectively. (b) The absorption and PL spectra of the CsPbBr₃ nanocrystal film at 6 K. The spectra of pump and probe spectra are also shown for references.

analyzed by a charge-coupled device (CCD) camera (Hamamatsu, S11071-1104). The overall spectral resolution is ~200 μeV . The pump beams were modulated by a chopper, while the probe beam (also as the local oscillator) was detected by the spectrometer to calculate $\Delta T/T_0$.⁰⁵ The T_0 denominator corresponds to the spectra due to probe laser only when pump beams are off. ΔT in the numerator relates to the difference of the probe spectra while pump beams are on vs off. The polarizations of the pump and probe beams are in a collinear scheme. The film samples were mounted in the cryostat (MicrostatHe, Oxford) with temperature calibrated with a sensor (DT-670C-SD, Lakeshore) mounted on the sample substrate.

Figure 1(b) shows the spectra of the pump and probe beams together with the absorption and photoluminescence spectra of the sample measured at 6 K. The pump NOPA is tuned to resonantly excite the band-edge transitions of the sample, while the probe beam is set with a broader spectral coverage. The pump spectrum was modified by a bandpass filter to meet the demand of undersampling to generate the 2DES spectra with high resolutions in energy domains. The excitation energy resolution is enabled by Fourier transformation of the signal in the time interval τ . The emission energy resolution, i.e., the Fourier transformation of the time interval between the third incident probe pulse and the signal t , is directly achieved by a spectrometer. The time interval between the second and the third pulses is population delay T corresponding to the population delay as commonly used for TA spectroscopy. By correlating the electronic transitions resonant to the excitation and emission photon energies, 2DES can disentangle inhomogeneous and homogeneous broadening along diagonal and orthogonal cross-diagonal directions, respectively.^{34–36}

III. RESULTS AND DISCUSSION

For nanocrystal ensembles, the intrinsic exciton linewidth is hidden by the entangled responses from nanocrystals of different sizes. Due to the diversity of the nanocrystal size, the linewidth of the photoluminescence spectrum of the CsPbBr₃ nanocrystal film at 6 K in Fig. 1(b) is ~ 30 meV, which is mainly caused by the inhomogeneous broadening. To characterize the intrinsic exciton homogeneous broadening and the underlying broadening mechanism of nanocrystal ensembles, we conduct 2DES measurements at cryogenic temperature.

Figure 2(a) shows the absorptive 2D spectra of CsPbBr₃ nanocrystals at 10 K at $T \sim 1$ ps featuring by a diagonal-elongated signal. This diagonally elongated signal is dominated by the different exciton resonant energies due to the size distribution of nanocrystals. By spectrally resolving the excitation and emission energy, the exciton homogeneous linewidth can be extracted from the orthogonal cross-diagonal sliced spectra in such a case of dominant inhomogeneity.³⁵ The extracted cross-diagonal spectrum is mainly featured by three peaks [Fig. 2(c)], i.e., two narrower peaks with an energy offset of 0 and 3.6 meV, respectively, and a broader peak ranging tens of meV. The peaks are consistent with the results in previous studies and were ascribed to the exciton broadening, the discrete optical phonon replica, and the coupled acoustic phonon continuum.^{28,34} By Lorentzian fitting, the exciton homogeneous linewidth γ is ~ 0.5 meV at 10 K, which is determined by the depopulation and the elastic-collision-induced pure dephasing processes.³⁷

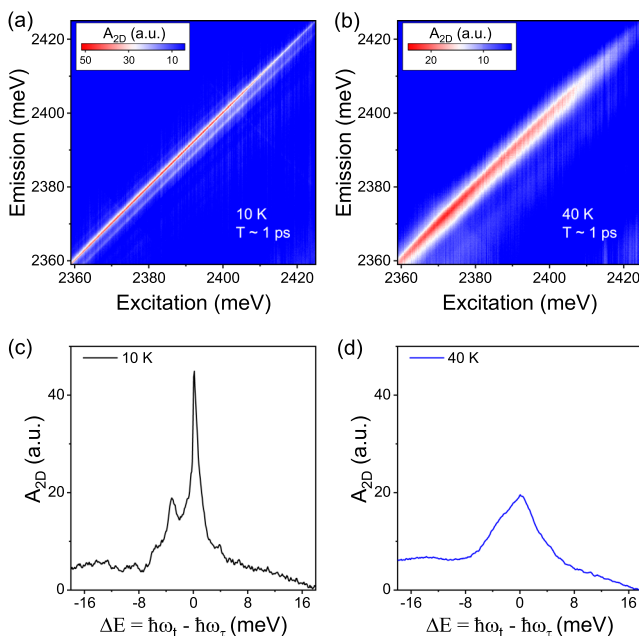


FIG. 2. Absorptive 2DES spectra measured at (a) 10 and (b) 40 K, respectively. The population time is set at 1 ps. The excitation density is $\sim 2.4 \mu\text{J}/\text{cm}^2$. Sliced cross-diagonal spectra extracted from 2D spectra at the temperature of (c) 10 and (d) 40 K with the center excitation photon energy at 2385 meV, respectively.

When temperature increases to 40 K, the diagonally elongated signal is significantly broadened as shown in Figs. 2(b) and 2(d). The exciton homogeneous linewidth γ at 40 K is ~ 1.9 meV, which is nearly four times as that at 10 K. Comparing the sliced cross-diagonal spectra at 10 and 40 K in Figs. 2(c) and 2(d), we find that the exciton linewidth and the phonon replica are obviously broadened with reduced peak intensity, which is consistent with the thermally induced dephasing due to elastic exciton–phonon scattering.^{37,38} Both of the sliced cross-diagonal spectra are featured with asymmetric pedestals due to the higher probability of emission than the absorption of vibrational energy.³⁴

To gain more insights about the thermally induced dephasing, we extract the sliced cross-diagonal spectra from 2D spectra measured at different temperatures [Fig. 3(a)]. With increasing temperature, the exciton peaks broaden to both high- and low-energy sides as a characteristic of exciton–phonon scattering. As investigated in previous studies,^{29,37,39,40} the linewidth of the exciton in semiconductors can be modeled by a temperature dependence as $\gamma(T) = \gamma_0 + aT + bN_{LO}(T)$, where the parameter γ_0 is the zero-temperature linewidth, a is the coupling strength between exciton and low-energy acoustic phonon modes (much smaller than $k_B T$), b is the coupling strength between exciton and discrete optical

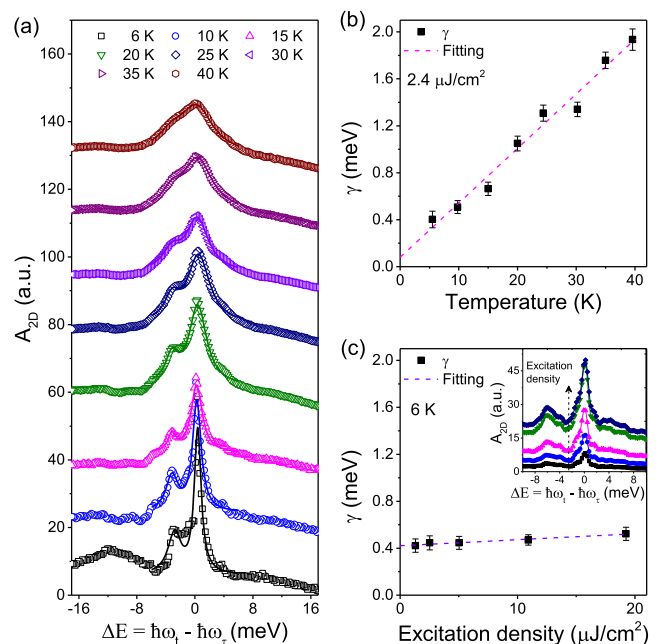


FIG. 3. (a) Sliced cross-diagonal spectra extracted from 2D spectra with center photon energy of 2385 meV recorded at different temperatures (the curves are shifted vertically for clarity). (b) The exciton homogeneous linewidth (black square) for temperatures ranging from 6 to 40 K. The dashed magenta line shows the linear fitting. The excitation density is set at $\sim 2.4 \mu\text{J}/\text{cm}^2$. The population time is set at 1 ps. (c) The exciton homogeneous linewidth (black square) for exciton densities ranging from 1.3 to $19.2 \mu\text{J}/\text{cm}^2$. The dashed purple line shows the linear fitting. The temperature is set at ~ 6 K. The inset shows the cross-diagonal spectral profile under different excitation densities. The population time is set at 0.5 ps.

phonon modes, and $N_{LO}(T) = 1/(\exp(E_{LO}/k_B T) - 1)$ represents the Bose distribution of phonons.^{29,37,39,40} The experimental data indicate that the exciton homogeneous linewidth γ increases proportionally with increasing temperature [Fig. 3(b)], which suggests the major contribution of the interaction between exciton and low-energy acoustic phonon modes to the exciton dephasing at low temperatures.^{29,40–42} By extrapolating the temperature dependence, we find that the zero-temperature linewidth γ_0 is $\sim 80 \mu\text{eV}$ corresponding to a dephasing time of ~ 8 ps. The slope of the linear relation a is $\sim 46 \mu\text{eV/K}$, which is comparable to the previous results in similar nanostructures.^{29,37,43}

In semiconductor quantum wells, the homogeneous linewidth is dependent on the excitation density due to exciton–exciton scattering.⁴⁴ Figure 3(c) shows the measured homogeneous linewidth at 6 K as a function of the excitation fluence in the range of 1.3–19.2 $\mu\text{J}/\text{cm}^2$. The exciton homogeneous linewidth γ shows no obvious fluence dependence, implying that the exciton–exciton scattering is not significant in the excitation density region. Such a behavior is possibly due to the fact that the excitation density is mainly in the single exciton regime. The average number of excitons per nanocrystals is less than 0.6 by multiplying the absorption cross section¹⁴ and the absorbed photon density at 19.2 $\mu\text{J}/\text{cm}^2$. Most nanocrystals are singly excited or unexcited, leading to insignificant no obvious dependence between exciton

homogeneous broadening and excitation density. In addition, the broad sideband induced by the coupling between exciton and low-energy acoustic phonon continuum was significantly enhanced with increasing excitation density [Fig. 3(c), inset], which is possibly caused by a higher carrier temperature upon increased excitation density.^{45–47}

Next, we analyze the influence of discrete optical phonon modes on the exciton dephasing. Single-nanocrystal studies have uncovered the multiple emission peaks due to the exciton fine-structure splitting and/or the phonon replica.^{48–50} As shown in Fig. 4(a), such discrete phonon replicas are also resolvable with off-diagonal features in 2D spectra, being manifested as beatings in the population time domain [Fig. 4(b), pink and orange lines]. The periods of these beating modes are extracted as ~ 1.13 and ~ 0.66 ps, respectively, which can be well fitted with a damped oscillation function (black lines), in agreement well with the two phonon modes of 29 cm^{-1} (3.6 meV) and 51 cm^{-1} (6.3 meV) as reported previously.^{28,49} These two optical phonon modes should arise from the Pb–Br–Pb bending motions.^{51–53} Both of the two beating modes can also be fitted at the diagonal peak [Fig. 4(b), the gray line and the fitted black line] with the same decay rate and opposite phase of the corresponding phonon peak. The distortion of the beating at the exciton peak can be induced by the existence of the polaronic exciton and/or coupling to other intrinsic phonon modes.^{43,51,54}

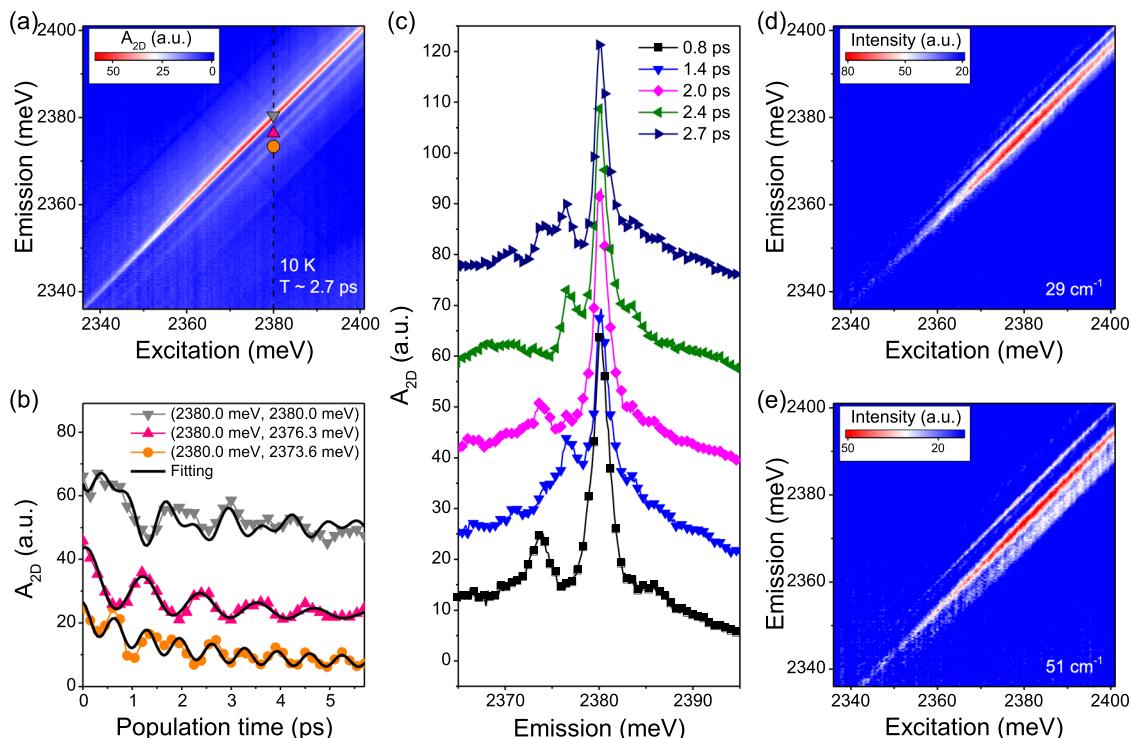


FIG. 4. (a) Absorptive 2D spectra measured at population time $T \sim 2.7$ ps under 10 K. (b) Temporal dynamics of the point marked in (a). The curves fitted with damped oscillation function are also shown as black lines to clarify the beating feature. The pink line is shifted for clarity. (c) The sliced emission spectra at the position marked in (a) with population time T as labeled showing the evolution of the discrete phonon sideband. The 2D maps of beating amplitudes in the domain of population delay are displayed for the wavenumbers (energies) of (d) 29 cm^{-1} (3.6 meV) and (e) 51 cm^{-1} (6.3 meV) corresponding to the two lower marked point in (a).

The coherent exciton–phonon interaction results in a strong dependence of the sliced cross-diagonal spectra on the population time delays [Fig. 4(c)]. For clarity, we show the beating maps at the wavenumbers of 29 and 51 cm^{-1} [Figs. 4(d) and 4(e)], respectively, where the off-diagonal beating amplitudes show elongated features in parallel to the diagonal features of excitonic resonance. The energy offsets are exactly the resonances of the phonon modes, confirming that the coherent exciton–optical phonon coupling induces phonon replicas in the optical transitions.

The exciton dephasing measured in this study is much faster in comparison with previous spectral analysis in single perovskite nanocrystals.^{25,28} The difference between 2DES and PL spectroscopies is a possible reason. For single-nanocrystal PL measurements, the low-lying emissive states are probed, while 2DES also probes the non-emissive states near band-edge. In addition, the exciton fine structures due to the reduced structural symmetry in different nanocrystals beyond the spectral resolution of the setup are also possibly responsible.^{27,48,49,55} For example, the exciton fine structure was found in CsPbI_3 nanocrystal ensembles via 2DES measurements by Liu *et al.*³¹ with energy splitting of the bright triplet exciton states of ~ 240 μeV at ~ 5 K. The summation of the bright fine structure may lead to a wider cross-diagonal peak. Moreover, the exciton spin flip process between the bright and the dark states may also contribute to exciton dephasing.^{27,56–58} In particular, the mixing between bright and dark states with slight energy differences may significantly increase the dephasing time. These features as uncovered by 2DES may not be probed in single dot PL measurements.³¹ Other than that, the shallow defect states may lead to additional channel of exciton dephasing.^{59,60}

IV. CONCLUSION

In summary, we have performed temperature-dependent 2DES measurements to characterize the exciton homogeneous linewidths in CsPbBr_3 nanocrystals. Experimental data suggest different roles played by the exciton–acoustic phonon and exciton–optical phonon interactions for exciton dephasing. The exciton–acoustic mode interaction makes the major contribution to the linewidth broadening at cryogenic temperature with a proportional temperature dependence in the range of 6–40 K. The exciton–optical mode interaction results in phonon replicas of excitonic transitions for two optical phonon modes of 29 and 51 cm^{-1} . Both of the acoustic and optical phonons can couple to excitons leading to sideband emission, which can influence the indistinguishability of photons in quantum light emitters.^{61,62} These findings provide insights about the excitonic linewidth broadening, i.e., dephasing time, which can limit the application of quantum light emitters. Suppressing the effect of electron–phonon interactions such as using an optical cavity to enhance the exciton emission can be helpful for the future design of perovskite nanocrystal-based quantum light emitters.⁶³

ACKNOWLEDGMENTS

This work was supported by the National Key R & D Program of China (Grant Nos. 2018YFA0209101 and 2017YFA0303700),

the National Natural Science Foundation of China (Grant Nos. 21922302, 21873047, 11904168, 91833305, 91850105, and 22033004), the Priority Academic Program Development of Jiangsu Higher Education Institutions (PAPD), and the Fundamental Research Funds for the Central University. The authors thank Dr. Xuewei Wu for providing technical assistance.

The authors declare no competing financial interest.

DATA AVAILABILITY

The data that support the findings of this study are available from the corresponding author upon reasonable request.

REFERENCES

- ¹M. Jeong, I. W. Choi, E. M. Go, Y. Cho, M. Kim, B. Lee, S. Jeong, Y. Jo, H. W. Choi, and J. Lee, “Stable perovskite solar cells with efficiency exceeding 24.8% and 0.3-V voltage loss,” *Science* **369**(6511), 1615–1620 (2020).
- ²R. Lin, K. Xiao, Z. Qin, Q. Han, C. Zhang, M. Wei, M. I. Saidaminov, Y. Gao, J. Xu, and M. Xiao, “Monolithic all-perovskite tandem solar cells with 24.8% efficiency exploiting comproportionation to suppress Sn(II) oxidation in precursor ink,” *Nat. Energy* **4**(10), 864–873 (2019).
- ³K. Xiao, R. Lin, Q. Han, Y. Hou, Z. Qin, H. T. Nguyen, J. Wen, M. Wei, V. Yeddu, and M. I. Saidaminov, “All-perovskite tandem solar cells with 24.2% certified efficiency and area over 1 cm^2 using surface-anchoring zwitterionic antioxidant,” *Nat. Energy* **5**, 870–880 (2020).
- ⁴J.-P. Correa-Baena, M. Saliba, T. Buonassisi, M. Grätzel, A. Abate, W. Tress, and A. Hagfeldt, “Promises and challenges of perovskite solar cells,” *Science* **358**(6364), 739–744 (2017).
- ⁵M. A. Green, A. Ho-Baillie, and H. J. Snaith, “The emergence of perovskite solar cells,” *Nat. Photonics* **8**(7), 506–514 (2014).
- ⁶N. K. Noel, S. D. Stranks, A. Abate, C. Wehrenfennig, S. Guarnera, A.-A. Haghighirad, A. Sadhanala, G. E. Eperon, S. K. Pathak, and M. B. Johnston, “Lead-free organic–inorganic tin halide perovskites for photovoltaic applications,” *Energy Environ. Sci.* **7**(9), 3061–3068 (2014).
- ⁷S. D. Stranks, G. E. Eperon, G. Grancini, C. Menelaou, M. J. P. Alcocer, T. Leijtens, L. M. Herz, A. Petrozza, and H. J. Snaith, “Electron–hole diffusion lengths exceeding 1 μm in an organometal trihalide perovskite absorber,” *Science* **342**(6156), 341–344 (2013).
- ⁸Q. Dong, Y. Fang, Y. Shao, P. Mulligan, J. Qiu, L. Cao, and J. Huang, “Electron–hole diffusion lengths >175 μm in solution-grown $\text{CH}_3\text{NH}_3\text{PbI}_3$ single crystals,” *Science* **347**(6225), 967–970 (2015).
- ⁹Z. Guo, Y. Wan, M. Yang, J. Snaider, K. Zhu, and L. Huang, “Long-range hot-carrier transport in hybrid perovskites visualized by ultrafast microscopy,” *Science* **356**(6333), 59–62 (2017).
- ¹⁰L. Protesescu, S. Yakunin, M. I. Bodnarchuk, F. Krieg, R. Caputo, C. H. Hendon, R. X. Yang, A. Walsh, and M. V. Kovalenko, “Nanocrystals of cesium lead halide perovskites (CsPbX_3 , X = Cl, Br, and I): Novel optoelectronic materials showing bright emission with wide color gamut,” *Nano Lett.* **15**(6), 3692–3696 (2015).
- ¹¹J. Shamsi, A. S. Urban, M. Imran, L. De Trizio, and L. Manna, “Metal halide perovskite nanocrystals: Synthesis, post-synthesis modifications, and their optical properties,” *Chem. Rev.* **119**(5), 3296–3348 (2019).
- ¹²L. Wang, L. Meng, L. Chen, S. Huang, X. Wu, G. Dai, L. Deng, J. Han, B. Zou, and C. Zhang, “Ultralow-threshold and color-tunable continuous-wave lasing at room-temperature from in situ fabricated perovskite quantum dots,” *J. Phys. Chem. Lett.* **10**(12), 3248–3253 (2019).
- ¹³Y. Xu, Q. Chen, C. Zhang, R. Wang, H. Wu, X. Zhang, G. Xing, W. W. Yu, X. Wang, Y. Zhang, and M. Xiao, “Two-photon-pumped perovskite semiconductor nanocrystal lasers,” *J. Am. Chem. Soc.* **138**(11), 3761–3768 (2016).
- ¹⁴S. Yakunin, L. Protesescu, F. Krieg, M. I. Bodnarchuk, G. Nedelcu, M. Humer, G. De Luca, M. Fiebig, W. Heiss, and M. V. Kovalenko, “Low-threshold amplified spontaneous emission and lasing from colloidal nanocrystals of caesium lead halide perovskites,” *Nat. Commun.* **6**, 8515 (2015).

- ¹⁵J. Chen, W. Du, J. Shi, M. Li, Y. Wang, Q. Zhang, and X. Liu, "Perovskite quantum dot lasers," *InfoMat* **2**(1), 170–183 (2019).
- ¹⁶X. Zhang, C. Sun, Y. Zhang, H. Wu, C. Ji, Y. Chuai, P. Wang, S. Wen, C. Zhang, and W. W. Yu, "Bright perovskite nanocrystal films for efficient light-emitting devices," *J. Phys. Chem. Lett.* **7**(22), 4602–4610 (2016).
- ¹⁷Y. Dong, Y.-K. Wang, F. Yuan, A. Johnston, Y. Liu, D. Ma, M.-J. Choi, B. Chen, M. Chekini, S.-W. Baek, L. K. Sagar, J. Fan, Y. Hou, M. Wu, S. Lee, B. Sun, S. Hoogland, R. Quintero-Bermudez, H. Ebe, P. Todorovic, F. Dinic, P. Li, H. T. Kung, M. I. Saidaminov, E. Kumacheva, E. Spiecker, L.-S. Liao, O. Voznyy, Z.-H. Lu, and E. H. Sargent, "Bipolar-shell resurfacing for blue LEDs based on strongly confined perovskite quantum dots," *Nat. Nanotechnol.* **15**(8), 668–674 (2020).
- ¹⁸J. Song, J. Li, X. Li, L. Xu, Y. Dong, and H. Zeng, "Quantum dot light-emitting diodes based on inorganic perovskite cesium lead halides (CsPbX₃)," *Adv. Mater.* **27**(44), 7162–7167 (2015).
- ¹⁹F. Zhang, H. Zhong, C. Chen, X.-g. Wu, X. Hu, H. Huang, J. Han, B. Zou, and Y. Dong, "Brightly luminescent and color-tunable colloidal CH₃NH₃PbX₃ (X = Br, I, Cl) quantum dots: Potential alternatives for display technology," *ACS Nano* **9**(4), 4533–4542 (2015).
- ²⁰F. Yan, S. T. Tan, X. Li, and H. V. Demir, "Light generation in lead halide perovskite nanocrystals: LEDs, color converters, lasers, and other applications," *Small* **15**(47), 1902079 (2019).
- ²¹Y.-S. Park, S. Guo, N. S. Makarov, and V. I. Klimov, "Room temperature single-photon emission from individual perovskite quantum dots," *ACS Nano* **9**(10), 10386–10393 (2015).
- ²²F. Hu, H. Zhang, C. Sun, C. Yin, B. Lv, C. Zhang, W. W. Yu, X. Wang, Y. Zhang, and M. Xiao, "Superior optical properties of perovskite nanocrystals as single photon emitters," *ACS Nano* **9**(12), 12410–12416 (2015).
- ²³F. Hu, C. Yin, H. Zhang, C. Sun, W. W. Yu, C. Zhang, X. Wang, Y. Zhang, and M. Xiao, "Slow Auger recombination of charged excitons in nonblinking perovskite nanocrystals without spectral diffusion," *Nano Lett.* **16**(10), 6425–6430 (2016).
- ²⁴B. Yu, C. Zhang, L. Chen, Z. Qin, X. Huang, X. Wang, and M. Xiao, "Ultrafast dynamics of photoexcited carriers in perovskite semiconductor nanocrystals," *Nanophotonics* (published online).
- ²⁵Y. Lv, C. Yin, C. Zhang, W. W. Yu, X. Wang, Y. Zhang, and M. Xiao, "Quantum interference in a single perovskite nanocrystal," *Nano Lett.* **19**(7), 4442–4447 (2019).
- ²⁶H. Utzat, W. Sun, A. E. K. Kaplan, F. Krieg, M. Ginterseder, B. Spokoyny, N. D. Klein, K. E. Shulenberg, C. F. Perkinson, M. V. Kovalenko, and M. G. Bawendi, "Coherent single-photon emission from colloidal lead halide perovskite quantum dots," *Science* **363**(6431), 1068–1072 (2019).
- ²⁷P. Tamarat, M. I. Bodnarchuk, J.-B. Trebbia, R. Erni, M. V. Kovalenko, J. Even, and B. Lounis, "The ground exciton state of formamidinium lead bromide perovskite nanocrystals is a singlet dark state," *Nat. Mater.* **18**(7), 717–724 (2019).
- ²⁸M. A. Becker, L. Scarpelli, G. Nedelcu, G. Rainò, F. Masia, P. Borri, T. Stöferle, M. V. Kovalenko, W. Langbein, and R. F. Mahrt, "Long exciton dephasing time and coherent phonon coupling in CsPbBr₂Cl perovskite nanocrystals," *Nano Lett.* **18**(12), 7546–7551 (2018).
- ²⁹A. Liu, G. Nagamine, L. G. Bonato, D. B. Almeida, L. F. Zagonel, A. F. Nogueira, L. A. Padilha, and S. T. Cundiff, "Towards engineering intrinsic linewidths and line-broadening in perovskite nanoplatelets," *arXiv:2011.02816* (2020).
- ³⁰X. Huang, L. Chen, C. Zhang, Z. Qin, B. Yu, X. Wang, and M. Xiao, "Inhomogeneous biexciton binding in perovskite semiconductor nanocrystals measured with two-dimensional spectroscopy," *J. Phys. Chem. Lett.* **11**(23), 10173–10181 (2020).
- ³¹A. Liu, D. B. Almeida, L. G. Bonato, G. Nagamine, L. F. Zagonel, A. F. Nogueira, L. A. Padilha, and S. T. Cundiff, "Multidimensional coherent spectroscopy reveals triplet state coherences in cesium lead-halide perovskite nanocrystals," *Sci. Adv.* **7**(1), eabb3594 (2021).
- ³²H. Seiler, S. Palato, C. Sonnichsen, H. Baker, E. Socie, D. P. Strandell, and P. Kambhampati, "Two-dimensional electronic spectroscopy reveals liquid-like line-shape dynamics in CsPbI₃ perovskite nanocrystals," *Nat. Commun.* **10**(1), 4962 (2019).
- ³³W. Zhu, R. Wang, C. Zhang, G. Wang, Y. Liu, W. Zhao, X. Dai, X. Wang, G. Cerullo, S. Cundiff, and M. Xiao, "Broadband two-dimensional electronic spectroscopy in an actively phase stabilized pump-probe configuration," *Opt. Express* **25**(18), 21115–21126 (2017).
- ³⁴A. Liu, D. B. Almeida, W.-K. Bae, L. A. Padilha, and S. T. Cundiff, "Simultaneous existence of confined and delocalized vibrational modes in colloidal quantum dots," *J. Phys. Chem. Lett.* **10**(20), 6144–6150 (2019).
- ³⁵M. E. Siemens, G. Moody, H. Li, A. D. Bristow, and S. T. Cundiff, "Resonance lineshapes in 2D FT spectroscopy," *Opt. Express* **18**, 17699 (2010).
- ³⁶A. Liu, D. B. Almeida, W. K. Bae, L. A. Padilha, and S. T. Cundiff, "Non-Markovian exciton-phonon interactions in core-shell colloidal quantum dots at femtosecond timescales," *Phys. Rev. Lett.* **123**(5), 057403 (2019).
- ³⁷G. Moody, C. Kavir Dass, K. Hao, C. H. Chen, L. J. Li, A. Singh, K. Tran, G. Clark, X. Xu, G. Berghauer, E. Malic, A. Knorr, and X. Li, "Intrinsic homogeneous linewidth and broadening mechanisms of excitons in monolayer transition metal dichalcogenides," *Nat. Commun.* **6**, 8315 (2015).
- ³⁸R. Singh, T. M. Autry, G. Nardin, G. Moody, H. Li, K. Pierz, M. Bieler, and S. T. Cundiff, "Anisotropic homogeneous linewidth of the heavy-hole exciton in (110)-oriented GaAs quantum wells," *Phys. Rev. B* **88**(4), 045304 (2013).
- ³⁹S. Rudin, T. L. Reinecke, and B. Segall, "Temperature-dependent exciton linewidths in semiconductors," *Phys. Rev. B* **42**(17), 11218–11231 (1990).
- ⁴⁰J. Lee, E. S. Koteles, and M. O. Vassell, "Luminescence linewidths of excitons in GaAs quantum wells below 150 K," *Phys. Rev. B* **33**(8), 5512–5516 (1986).
- ⁴¹L. Hou, P. Tamarat, and B. Lounis, "Revealing the exciton fine structure in lead halide perovskite nanocrystals," *Nanomaterials* **11**(4), 1058 (2021).
- ⁴²E. A. Muljarov and R. Zimmermann, "Dephasing in quantum dots: Quadratic coupling to acoustic phonons," *Phys. Rev. Lett.* **93**(23), 237401 (2004).
- ⁴³F. Thouin, D. Cortecchia, A. Petrozza, A. R. Srimath Kandada, and C. Silva, "Enhanced screening and spectral diversity in many-body elastic scattering of excitons in two-dimensional hybrid metal-halide perovskites," *Phys. Rev. Res.* **1**(3), 032032 (2019).
- ⁴⁴J. M. Shacklette and S. T. Cundiff, "Role of excitation-induced shift in the coherent optical response of semiconductors," *Phys. Rev. B* **66**(4), 045309 (2002).
- ⁴⁵Y. Yang, D. P. Ostrowski, R. M. France, K. Zhu, J. van de Lagemaat, J. M. Luther, and M. C. Beard, "Observation of a hot-phonon bottleneck in lead-iodide perovskites," *Nat. Photonics* **10**(1), 53–59 (2015).
- ⁴⁶B. Yu, L. Chen, Z. Qu, C. Zhang, Z. Qin, X. Wang, and M. Xiao, "Size-dependent hot carrier dynamics in perovskite nanocrystals revealed by two-dimensional electronic spectroscopy," *J. Phys. Chem. Lett.* **12**(1), 238–244 (2021).
- ⁴⁷B. T. Diroll and R. D. Schaller, "Intraband cooling in all-inorganic and hybrid organic-inorganic perovskite nanocrystals," *Adv. Funct. Mater.* **29**(37), 1901725 (2019).
- ⁴⁸C. Yin, L. Chen, N. Song, Y. Lv, F. Hu, C. Sun, W. W. Yu, C. Zhang, X. Wang, Y. Zhang, and M. Xiao, "Bright-exciton fine-structure splittings in single perovskite nanocrystals," *Phys. Rev. Lett.* **119**(2), 026401 (2017).
- ⁴⁹M. Fu, P. Tamarat, H. Huang, J. Even, A. L. Rogach, and B. Lounis, "Neutral and charged exciton fine structure in single lead halide perovskite nanocrystals revealed by magneto-optical spectroscopy," *Nano Lett.* **17**(5), 2895–2901 (2017).
- ⁵⁰M. Fu, P. Tamarat, J. B. Trebbia, M. I. Bodnarchuk, M. V. Kovalenko, J. Even, and B. Lounis, "Unraveling exciton-phonon coupling in individual FAPbI₃ nanocrystals emitting near-infrared single photons," *Nat. Commun.* **9**(1), 3318 (2018).
- ⁵¹F. Thouin, D. A. Valverde-Chávez, C. Quarti, D. Cortecchia, I. Bargigia, D. Beljonne, A. Petrozza, C. Silva, and A. R. Srimath Kandada, "Phonon coherences reveal the polaronic character of excitons in two-dimensional lead halide perovskites," *Nat. Mater.* **18**(4), 349–356 (2019).
- ⁵²K. Miyata, D. Meggiolaro, M. T. Trinh, P. P. Joshi, E. Mosconi, S. C. Jones, F. De Angelis, and X.-Y. Zhu, "Large polarons in lead halide perovskites," *Sci. Adv.* **3**(8), e1701217 (2017).
- ⁵³W. Zhao, Z. Qin, C. Zhang, G. Wang, X. Dai, and M. Xiao, "Coherent exciton-phonon coupling in perovskite semiconductor nanocrystals studied by two-dimensional electronic spectroscopy," *Appl. Phys. Lett.* **115**(24), 243101 (2019).
- ⁵⁴S. Neutzner, F. Thouin, D. Cortecchia, A. Petrozza, C. Silva, and A. R. Srimath Kandada, "Exciton-polaron spectral structures in two-dimensional hybrid lead-halide perovskites," *Phys. Rev. Mater.* **2**(6), 064605 (2018).

- ⁵⁵C. Yin, Y. Lv, X. Zhang, Y. Zhang, W. W. Yu, C. Zhang, Z.-G. Yu, X. Wang, and M. Xiao, "Transition from doublet to triplet excitons in single perovskite nanocrystals," *J. Phys. Chem. Lett.* **11**(14), 5750–5755 (2020).
- ⁵⁶L. Chen, B. Li, C. Zhang, X. Huang, X. Wang, and M. Xiao, "Composition-dependent energy splitting between bright and dark excitons in lead halide perovskite nanocrystals," *Nano Lett.* **18**(3), 2074–2080 (2018).
- ⁵⁷F. Masia, N. Accanto, W. Langbein, and P. Borri, "Spin-flip limited exciton dephasing in CdSe/ZnS colloidal quantum dots," *Phys. Rev. Lett.* **108**(8), 087401 (2012).
- ⁵⁸N. Accanto, F. Masia, I. Moreels, Z. Hens, W. Langbein, and P. Borri, "Engineering the spin-flip limited exciton dephasing in colloidal CdSe/CdS quantum dots," *ACS Nano* **6**, 5227–5233 (2012).
- ⁵⁹B. F. Habenicht, H. Kamisaka, K. Yamashita, and O. V. Prezhdo, "Ab initio study of vibrational dephasing of electronic excitations in semiconducting carbon nanotubes," *Nano Lett.* **7**(11), 3260–3265 (2007).
- ⁶⁰A. Liu, L. G. Bonato, F. Sessa, D. B. Almeida, E. Isele, G. Nagamine, L. F. Zagonel, A. F. Nogueira, L. A. Padilha, and S. T. Cundiff, "Effect of dimensionality on the optical absorption properties of CsPbI₃ perovskite nanocrystals," *J. Chem. Phys.* **151**(19), 191103 (2019).
- ⁶¹A. J. Brash, J. Iles-Smith, C. L. Phillips, D. P. S. McCutcheon, J. O'Hara, E. Clarke, B. Royall, L. R. Wilson, J. Mork, M. S. Skolnick, A. M. Fox, and A. Nazir, "Light scattering from solid-state quantum emitters: Beyond the atomic picture," *Phys. Rev. Lett.* **123**(16), 167403 (2019).
- ⁶²J. Iles-Smith, D. P. S. McCutcheon, A. Nazir, and J. Mørk, "Phonon scattering inhibits simultaneous near-unity efficiency and indistinguishability in semiconductor single-photon sources," *Nat. Photonics* **11**(8), 521–526 (2017).
- ⁶³T. Grange, N. Somaschi, C. Anton, L. De Santis, G. Coppola, V. Giesz, A. Lemaitre, I. Sagnes, A. Auffeves, and P. Senellart, "Reducing phonon-induced decoherence in solid-state single-photon sources with cavity quantum electrodynamics," *Phys. Rev. Lett.* **118**(25), 253602 (2017).